Influence of surfactant on drop deformation in an electric field

Knut Erik Teigen[1, a)] and Svend Tollak Munkejord[2, b)]
[1)]*Department of Energy and Process Engineering, Norwegian University of Science and Technology (NTNU), NO-7491 Trondheim, Norway*
[2)]*SINTEF Energy Research, P.O. Box 4761 Sluppen, NO-7465 Trondheim, Norway*

The deformation of a surfactant-covered, viscous drop suspended in a viscous fluid under the influence of an electric field is investigated using numerical simulations. The full Navier–Stokes equations are solved in both fluid phases, and the motion of the interface and the interfacial discontinuities are handled using the level-set method. The leaky-dielectric model is used to take into account the effect of an electric field. The surfactant is assumed to be insoluble, and an evolution equation for the motion of surfactant is solved along the drop surface. The surfactant concentration and the interfacial tension are coupled through a non-linear equation of state.

The numerical results show that the effect of surfactant strongly depends on the relative permittivity and conductivity between the fluids. The presence of surfactant can both increase and reduce the deformation, depending on the shape of the deformation and the direction of the electrically induced circulation.

PACS numbers: 47.11.-j, 47.65.-d, 47.55.D-, 47.55.dk
Keywords: Drop deformation, two-phase flow, electrohydrodynamics, surfactant

I. INTRODUCTION

Electric fields are used to manipulate drops in several industrial applications. These include taking advantage of induced circulation to promote heat transfer in heat exchangers[1] and increasing the coalescence rate between water drops to enhance demulsification in crude oils[2]. It is common for such fluid systems to contain surface-active agents (surfactants), either naturally present as impurities or deliberately added to modify the properties of the system. For the case of demulsification of crude oils, crude oils contain natural surfactants such as asphaltenes, resins, waxes and naphthenic acids[3], but surfactants are also added to the system to act as a demulsifier.

The effect of surfactants on the steady-state deformation of a drop has been studied by, among others, Milliken *et al.* [4], Pawar and Stebe [5] and Eggleton and Stebe [6], Eggleton *et al.* [7] for a drop in extensional flow and by Li and Pozrikidis [8] and Lai *et al.* [9] for a drop in shear flow. Due to the external flow, surfactant will be swept to the tips of the drop. This gives rise to gradients in the interfacial tension which causes stresses tangential to the surface, often denoted Marangoni stresses, that try to redistribute the surfactant. The convection of surfactant gives a higher interfacial tension at the middle of the drop and a lower interfacial tension at the tips compared to a clean surface, which promotes a higher deformation. On the other hand, as the drop is stretched, the surfactant concentration is diluted due to the increase in interfacial area. For high Marangoni stresses, the interfacial tension can increase over the entire drop, and this dilatation can reduce deformation compared to a clean drop. For relatively dilute surfactant concentrations, the Marangoni stresses are low, so that the first effect dominates, and the deformation is larger than that of a clean drop. For very high surfactant concentrations, however, a small non-uniformity in surfactant gives rise to large Marangoni stresses, and the effect of dilatation becomes dominant, resulting in lower deformation compared to a clean drop. The influence of surfactants on breakup has been studied among others by Milliken *et al.* [4] and Eggleton *et al.* [10] for a drop in extensional flow and by De Bruijn [11] and Renardy *et al.* [12] for a drop in shear flow. It was observed that for dilute concentrations of surfactants, tip-streaming would occur, where the drop tips would become highly curved and emit small drops. In Teigen *et al.* [13], surfactant solubility was also found to have an appreciable influence on the breakup dynamics.

When the velocity field is induced by an electric field as opposed to externally applied through e.g. a shear flow, we may expect the drop behavior to be different. Of particular interest is the fact that a drop in an electric field may deform into either a prolate shape or an oblate shape depending on the electrical properties of the fluid system[14,15]. For the case of prolate deformation, the induced circulation can in addition run both from pole to equator and vice-versa, which will obviously affect the deformation when a surfactant is present.

To the authors' knowledge, the only study of the combined effect of electric fields and surfactants is by Ha and Yang [16]. They demonstrated that for a relatively highly conducting drop, the change in deformation is only due to a uniform lowering of interfacial tension. This is not surprising, since for such a conductive drop, the electric field lines will be close to perpendicular to the drop interface, and the electric field inside the drop will be close to zero. Hence, the drop is unable to support a tangential stress and as the drop reaches a steady state the induced flow will tend to zero. The surfactant will eventually redistribute itself due to diffusion and the deformation will become equal to that of a clean surface (given the proper scaling of the electric field strength). For a leaky-dielectric system in which the drop deformed into an oblate shape, however, it was found that the presence of surfactant gave a larger deformation than that of a clean surface.

The aim of this work is to study the deformation of a surfactant-covered drop in an electric field using numerical simulations. In Section II we give the mathematical formula-

[a)]Electronic mail: knut.erik.teigen@ntnu.no, knutert@gmail.com
[b)]Electronic mail: svend.t.munkejord@sintef.no

tion of the problem and present our numerical method. In Section III we validate the method and investigate the steady-state deformation for different configurations of electrical properties and the influence of surfactants. Concluding remarks and proposals for future work are given in Section V.

II. MATHEMATICAL MODEL AND NUMERICAL METHOD

A. The level-set method

We consider a system of two immiscible phases separated by an interface, Γ. We use the level-set method[17,18] to capture this interface, which allows handling of the discontinuities at the interface in a simple and accurate manner.

In the level-set method, the interface is defined implicitly by the zero level set

$$\Gamma = \{\boldsymbol{x} | \phi(\boldsymbol{x}, t) = 0\}, \tag{1}$$

where ϕ is the level-set function, which denotes the signed distance to the interface. The level-set function moves with the interface velocity $\boldsymbol{u}_{\text{int}}$ according to

$$\frac{\partial \phi}{\partial t} + \boldsymbol{u} \cdot \nabla \phi = 0. \tag{2}$$

The standard level-set reinitialization procedure is used to keep the level-set function as a signed distance function throughout the computation. This is accomplished by solving

$$\begin{aligned} \frac{\partial \phi}{\partial \tau} + S(\phi_0)(|\nabla \phi| - 1) = 0, \\ \phi(\boldsymbol{x}, 0) = \phi_0(\boldsymbol{x}). \end{aligned} \tag{3}$$

Reinitialization is performed every other time step.

With the level-set function as a signed distance function, the normal vector (inward) can be calculated as

$$\boldsymbol{n} = \frac{\nabla \phi}{|\nabla \phi|}, \tag{4}$$

and the curvature as

$$\kappa = -\nabla \cdot \left(\frac{\nabla \phi}{|\nabla \phi|} \right). \tag{5}$$

The density, ρ, viscosity, μ, permittivity, ε, and conductivity, σ, are discontinuous across the interface. We smooth these properties over a narrow transition region using

$$\rho(H_\Gamma) = \rho_1 H_\Gamma + (1 - H_\Gamma)\rho_2, \tag{6}$$

$$\mu(H_\Gamma) = \mu_1 H_\Gamma + (1 - H_\Gamma)\mu_2, \tag{7}$$

$$\frac{1}{\varepsilon} = \frac{H_\Gamma}{\varepsilon_1} + \frac{1 - H_\Gamma}{\varepsilon_2}, \tag{8}$$

$$\frac{1}{\sigma} = \frac{H_\Gamma}{\sigma_1} + \frac{1 - H_\Gamma}{\sigma_2}, \tag{9}$$

where H_Γ is the regularized Heaviside function, defined as

$$H_\Gamma(\phi) = \begin{cases} 0 & \phi < -\epsilon \\ \frac{1}{2} + \frac{\phi}{2\epsilon} + \frac{1}{2\pi} \sin\left(\frac{\pi \phi}{\epsilon}\right) & |\phi| \leq \epsilon \\ 1 & \phi > \epsilon. \end{cases} \tag{10}$$

Here, ϵ is the smearing width. We employ a smearing width of $\epsilon = 1.5h$, where h is the grid spacing.

It was shown by Tomar *et al.* [19] that using a harmonic mean for the electrical properties was beneficial over an arithmetic mean.

We also define the regularized surface delta function,

$$\delta_\Gamma(\phi) = \begin{cases} 0 & |\phi| < \epsilon \\ \frac{1}{2\epsilon}\left(1 + \cos\frac{\pi \phi}{\epsilon}\right) & |\phi| \geq \epsilon. \end{cases} \tag{11}$$

B. Governing equations for the flow

We assume that the flow is governed by the axisymmetric Navier–Stokes equations in each phase, with additional terms accounting for interfacial-tension forces and electric forces. The Navier–Stokes equations are

$$\begin{aligned} \rho\left(\frac{\partial \boldsymbol{u}}{\partial t} + (\boldsymbol{u} \cdot \nabla)\boldsymbol{u}\right) = -\nabla p + \nabla \cdot [\mu(\nabla \boldsymbol{u} + \nabla \boldsymbol{u}^T)] \\ + \boldsymbol{f}_c + \boldsymbol{f}_e, \\ \nabla \cdot \boldsymbol{u} = 0, \end{aligned} \tag{12}$$

where ρ is the density, $\boldsymbol{u}$ is the velocity, p is the pressure, μ is the dynamic viscosity, $\boldsymbol{f}_c$ is the capillary force and $\boldsymbol{f}_e$ is the electric force. The capillary force is given by the divergence of the capillary-pressure tensor, F_c:

$$\boldsymbol{f}_c = \nabla \cdot \mathsf{F}_c = \gamma \kappa \nabla H_\Gamma - (\nabla_\Gamma \gamma)\delta_\Gamma. \tag{13}$$

Here, γ is the interfacial tension, δ_Γ is the regularized delta function, I is the identity tensor, $\boldsymbol{n}$ is the inward-pointing normal vector, κ is the mean curvature and $\nabla_\Gamma = (I - \boldsymbol{n} \otimes \boldsymbol{n})\nabla$ the surface-gradient operator.

The electric force is given by the divergence of the Maxwell stress tensor, $\boldsymbol{f}_e = \nabla \cdot M$, where

$$M = \varepsilon \left[\boldsymbol{E}\boldsymbol{E} - \frac{1}{2}(\boldsymbol{E} \cdot \boldsymbol{E})I \right]. \tag{14}$$

Here, $\boldsymbol{E}$ is the electric field. We assume that the fluids are leaky dielectric. That is, we assume that the volume charges reach steady state in a much shorter time than the fluid. This means that charges accumulate on the interface almost instantly, and the equation for charge conservation,

$$\frac{\mathrm{D}q_v}{\mathrm{D}t} + \nabla \cdot \boldsymbol{J} = 0, \tag{15}$$

where $\boldsymbol{J} = \sigma \boldsymbol{E}$ is the current density, can be simplified to

$$\nabla \cdot \boldsymbol{J} = \nabla \cdot (\sigma \boldsymbol{E}) = 0, \tag{16}$$

where σ is the conductivity. Because the electric field is divergence free, this can be written as

$$\nabla \cdot (\sigma \nabla \Psi) = 0, \tag{17}$$

where Ψ is the electric potential.

We do not calculate the Maxwell tensor directly, but instead calculate the electric force using an equivalent volume-force representation given by

$$\boldsymbol{f}_e = -\frac{1}{2}(\boldsymbol{E} \cdot \boldsymbol{E})\nabla \varepsilon + q_v \boldsymbol{E}, \tag{18}$$

where $q_v = \nabla \cdot (\varepsilon \boldsymbol{E})$ is the volume-charge density.

Next, we assume that there is an insoluble surfactant present on the interface, which modifies the interfacial tension. Here, we follow the approach introduced by Xu and Zhao [20] and Xu *et al.* [21], who developed a method for treating surfactants using the level-set method. The dynamics of the surfactant concentration, f, is governed by[20,21]

$$\begin{aligned} &\frac{\partial f}{\partial t} + \boldsymbol{u} \cdot \nabla f - \boldsymbol{n} \cdot \nabla \boldsymbol{u} \cdot \boldsymbol{n} f \\ &\quad = D_f \left(\nabla^2 f - \boldsymbol{n} \cdot \nabla \nabla \cdot \boldsymbol{n} f + \kappa (\boldsymbol{n} \cdot \nabla f) \right), \end{aligned} \tag{19}$$

where D_f is the surfactant diffusion coefficient. We employ the Langmuir equation of state to relate the interfacial tension and surfactant concentration,

$$\gamma(f) = \gamma_0 \left[1 + \beta \ln \left(1 - \frac{f}{f_\infty} \right) \right]. \tag{20}$$

Here, $\beta = \bar{R} T f_\infty / \gamma_0$ is the surface elasticity number, and f_∞ is the maximum surfactant packing. $\bar{R}$ is the universal gas constant, T the temperature and γ_0 is the interfacial tension of the clean surface.

Since we assume that the surfactant is insoluble, it is only defined on the interface. In order to solve the evolution equation numerically, we must therefore first extend the surfactant concentration off the interface[22]. We do this by solving the equation[23]

$$\frac{\partial f}{\partial \tau} + S(\phi_0) \boldsymbol{n} \cdot \nabla f = 0, \tag{21}$$

where S is a sign function given by

$$S(\phi) = \frac{\phi}{\sqrt{\phi^2 + 2\Delta x^2}}. \tag{22}$$

C. Non-dimensionalization

We solve the above equations in their dimensional form, but express the results in terms of relevant non-dimensional quantities. To cast the mathematical model in nondimensional form, we introduce the following nondimensional variables, denoted with a $*$,

$$x^* = \frac{x}{R}, \qquad t^* = \sqrt{\frac{\gamma_e}{\rho_2 R^3}} t, \qquad \boldsymbol{u}^* = \boldsymbol{u} \sqrt{\frac{\rho_2 R}{\gamma_e}}, \tag{23}$$

$$p^* = \frac{pR}{\gamma_e}, \qquad \rho^* = \frac{\rho}{\rho_2}, \qquad \mu^* = \frac{\mu}{\mu_2}, \tag{24}$$

$$f^* = \frac{f}{f_\infty}, \qquad \kappa^* = \kappa R, \qquad \varepsilon^* = \frac{\varepsilon}{\varepsilon_2}, \tag{25}$$

$$\sigma^* = \frac{\sigma}{\sigma_2} \qquad \gamma^* = \frac{\gamma}{\gamma_e}, \qquad \boldsymbol{E}^* = \frac{\boldsymbol{E}}{E_\infty}. \tag{26}$$

Here, the time scale is based on the frequency of a freely oscillating drop of radius R, and the pressure scale is based on the capillary pressure. Subscript 2 denotes the continuous phase. The electric field scale, E_∞, is found by dividing the potential difference by the domain height. The interfacial tension is scaled by the equilibrium interfacial tension, denoted by subscript e. This means that only the effect of a non-uniform interfacial tension is highlighted, and not the effect of a uniform lowering of the interfacial tension.

The above scalings yield the Navier–Stokes equations as

$$\begin{aligned} \rho^* \left(\frac{\partial \boldsymbol{u}^*}{\partial t^*} + (\boldsymbol{u}^* \cdot \nabla) \boldsymbol{u}^* \right) &= -\nabla p^* \\ &\quad + Oh \nabla \cdot [\mu^* (\nabla \boldsymbol{u}^* + \nabla \boldsymbol{u}^{*T})] \\ &\quad + \boldsymbol{f}_c^* + Ca_E \boldsymbol{f}_e^* \\ \nabla \cdot \boldsymbol{u}^* &= 0, \end{aligned} \tag{27}$$

where $\boldsymbol{f}_c^*$ and $\boldsymbol{f}_e^*$ are equivalent to $\boldsymbol{f}_c$ and $\boldsymbol{f}_e$, only with dimensionless quantities. Two dimensionless quantities appear, the Ohnesorge number, $Oh = \mu_2 / \sqrt{\rho_2 \gamma_e R}$, which indicates the ratio of viscous force to interfacial-tension force, and the electric capillary number, $Ca_E = \varepsilon_2 R (\boldsymbol{E} \cdot \boldsymbol{E})_\infty / \gamma_e$, which is the dimensionless strength of the external electric field.

The equation for the electric potential becomes

$$\nabla \cdot (\sigma^* \nabla \Psi^*) = 0, \tag{28}$$

and the surfactant equation becomes

$$\begin{aligned} &\frac{\partial f^*}{\partial t} + \boldsymbol{u}^* \cdot \nabla f^* - \boldsymbol{n} \cdot \nabla \boldsymbol{u}^* \cdot \boldsymbol{n} f^* \\ &\quad = \frac{1}{Pe} \left(\nabla^2 f^* - \boldsymbol{n} \cdot \nabla \nabla \cdot \boldsymbol{n} f^* + \kappa^* (\boldsymbol{n} \cdot \nabla f^*) \right), \end{aligned} \tag{29}$$

where $Pe = RU/D_f$ is the surface Peclet number.

Henceforth we will omit the superscript $*$ for the non-dimensional quantities.

D. Numerical method

The equations are spatially discretized on a Cartesian staggered grid, with scalar values stored in cell centers and vector values stored at cell boundaries. The convective terms are discretized using the fifth order Weighted Essentially Non-Oscillatory (WENO) scheme[24], and viscous terms are discretized using standard second-order central differences.

A second-order projection scheme is used to solve the Navier–Stokes equations. First, a temporary vector field, $\boldsymbol{a}$, is calculated:

$$\begin{aligned}\boldsymbol{a} = &-(\boldsymbol{u}\cdot\nabla)\boldsymbol{u} + Oh\nabla\cdot[\mu(\nabla\boldsymbol{u}+\nabla\boldsymbol{u}^T)] \\ &+ \boldsymbol{f}_c + Ca_E\boldsymbol{f}_e.\end{aligned} \tag{30}$$

Then the pressure is found by solving

$$\nabla\cdot\left(\frac{\nabla p}{\rho}\right) = \nabla\cdot\boldsymbol{a}. \tag{31}$$

Finally, the velocity field is calculated with

$$\frac{\partial\boldsymbol{u}}{\partial t} = \boldsymbol{a} - \frac{\nabla p}{\rho}. \tag{32}$$

The evolution in time is calculated using a four-step third-order, strong stability-preserving (SSP) Runge-Kutta (RK) method[25,26]. This method is also used for the level-set equation and the surfactant equation, while a four-step second-order SSP-RK method is employed for the reinitialization of the level-set equation and extrapolation of surfactant.

One substep in the main RK solver can be summarized as follows:

1. Solve Eq. (17) for the electric potential and find the electric field.
2. Calculate electric forces using Eq. (18).
3. Find the interfacial tension using Eq. (20) and calculate interfacial-tension forces with Eq. (13).
4. Calculate $\boldsymbol{a}$ using Eq. (30) and solve Eq. (31) for pressure.
5. Calculate the rate of change of the level-set function using Eq. (2).
6. Extrapolate the surfactant concentration by solving Eq (21).
7. Calculate the rate of change of the surfactant concentration using Eq. (19).

III. RESULTS AND DISCUSSION

We first present a comparison with theoretical results for the steady-state deformation of a clean drop to validate our implementation and establish a frame of reference for the simulation with surfactants. Then, we present results for the steady-state deformation of a surfactant-covered drop for various electrical properties. Finally, we discuss the influence of surfactants on the transient deformation of a conductive drop when the electric field is so high that no steady-state solution exists.

The computational domain is illustrated in Fig. 1. The simulations are performed in an axisymmetric, cylindrical coordinate system, where the axis of symmetry is aligned with the electric field. Additionally, it is assumed that the fluid mechanics are symmetric about the r-axis, while the electric problem is anti-symmetric. This means that the simulations are only performed in one quadrant of the drop, which reduces the computational complexity. The domain size was $4R\times 4R$, and the grid spacing was $h = R/20$. Since we use a transient numerical method, we stop the simulation when the relative change in deformation from one time step to the next is less than 1×10^{-4}.

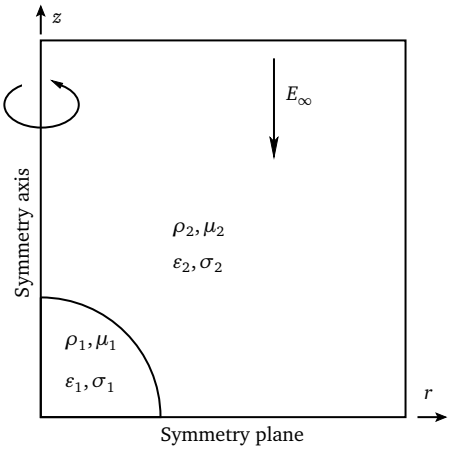

FIG. 1. Illustration of the computational domain.

An issue with level-set simulations is mass conservation. Since the simulation times in this work are short and a relatively fine grid is used, the mass loss is kept low. We also use a more consistent formulation of the capillary surface force[27],

$$\boldsymbol{f}_{\text{capillary}} = \gamma\kappa\nabla H_\Gamma, \tag{33}$$

instead of the often cited

$$\boldsymbol{f}_{\text{capillary}} = \gamma\kappa\delta_\Gamma\boldsymbol{n}. \tag{34}$$

This significantly improves mass conservation. We ensured that for all the simulations presented here, the change in mass for both fluid and surfactant was less than 1 %.

A. Code validation

In this section, the code is validated by comparison to small-deformation theory and other numerical results from the literature.

1. Validation of electric force

In the limit of small perturbations, an expression for the deformation of a leaky-dielectric drop in a leaky-dielectric medium was derived by Taylor [14] to the first order, and later extended to second order by Ajayi [28]. This can be written as

$$D = \frac{b-a}{b+a} = k_1 Ca_E + k_2 Ca_E^2, \tag{35}$$

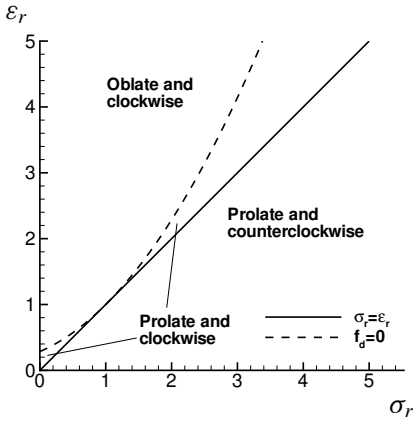

FIG. 2. A map of the different induced flow patterns and deformations for $\mu_r = 1$.

where a and b are the drop extensions along the r-axis and z-axis, respectively. The coefficients k_1 and k_2 are given by

$$
\begin{aligned}
k_1 &= \frac{9}{16}\frac{\sigma_r^2}{(2+\sigma_r)^2} f_d, \\
k_2 &= \frac{(139\sigma_r - 154)\sigma_r^2 f_d + (\sigma_r^2 + 2\sigma_r - \sigma_r\varepsilon_r - 2\varepsilon_r)80\beta}{80(2+\sigma_r)^3} k_1, \\
f_d &= \frac{\sigma_r^2 - 2\sigma_r + 1 + (\sigma_r - \varepsilon_r)\left[2 + \frac{3}{5}\frac{2+3\mu_r}{1+\mu_r}\right]}{\sigma_r^2}, \\
\beta &= \frac{23}{20} - \frac{139}{210}\frac{1-\mu_r}{1+\mu_r} - \frac{27}{700}\left(\frac{1-\mu_r}{1+\mu_r}\right).
\end{aligned}
\tag{36}
$$

Here, subscript r denotes the ratio between phase 1 and phase 2. The form of deformation is given by f_d. If $f_d > 0$, the drop will have a prolate shape. If $f_d < 0$, the shape will be oblate. If $\varepsilon_r < \sigma_r$, then $f_d > 0$ and the deformation will always be prolate. For $\varepsilon_r > \sigma_r$, however, both kinds of deformation may occur. Additionally, when the deformation is oblate, the induced flow pattern is always clockwise in the first quadrant of the drop. For the prolate shape, the flow can be both clockwise and counterclockwise. A map of these situations is given in Fig. 2.

Simulations of four different configurations were performed at various electric capillary numbers and compared to Eq. (35). The different configurations were chosen to correspond to the different deformation types and flow patterns given in Fig. 2, and are summarized in Table I. The viscosity ratio is set to unity.

The results are shown in Fig. 3. For small Ca_E, the numerical simulations are in good agreement with the first-order theory, while for higher numbers, they start to deviate. This behavior is expected since the theory is only valid for small deformations, and our results are in line with other numerical investigations[19,29,30]. The second-order theory is a better match to the simulations, which was also observed by Lac and Homsy [31].

The drop morphology along with induced flow patterns for $Ca_E = 0.4$ are shown in Fig. 4. We see that for case A, the flow is from equator to pole, while for cases B and C, the flow is from pole to equator. These patterns match those predicted from the theory.

TABLE I. The parameters used for validation of the electric forces, together with the predicted deformation types and flow patterns. C=Clockwise, CC=Counterclockwise.

Case	σ_r	ε_r	f_d	Deformation	Flow pattern
A	3	1	1.22	Prolate	CC
B	3	3.5	0.25	Prolate	C
C	1	2	-3.50	Oblate	C
D	2	2.2857	0.00	None	C

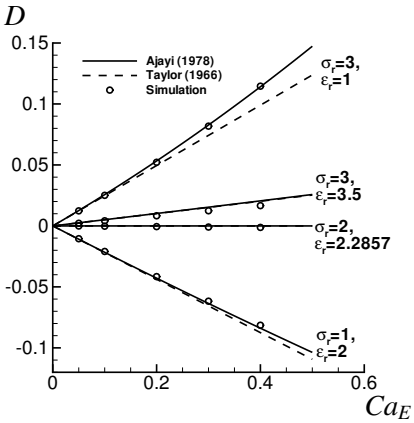

FIG. 3. Comparison of numerical results (circles) and the small deformation theory of Taylor [14] (dashed lines) and Ajayi [28] (solid lines) for the parameters given in Table I.

2. Validation of Marangoni force

Here we consider a surfactant-covered drop in a velocity field given by $\boldsymbol{u} = G(-r/2, z)$, and no electric field. An expression for the resulting deformation was derived by Stone and Leal [32] under the assumptions $Ca = \mu_2 GR/\gamma_0 \ll 1$, $Pe \ll 1$ and $\mu_r = O(1)$. This can be written as

$$D \approx \frac{3Cab_r}{4 + Cab_r}, \tag{37}$$

$$b_r = \frac{(80 + 95\mu_r) + \frac{4\beta Pe}{Ca(1-\beta)}}{40(1+\mu_r) + \frac{2\beta Pe}{Ca(1-\beta)}}. \tag{38}$$

Here, we set the viscosity ratio to $\mu_r = 1$ and the surfactant parameters are $Pe = 0.1$ and $\beta = 0.5$.

Fig. 5 shows the simulated results together with Eq. (37) and results from Stone and Leal [32] where they used the boundary-integral method to simulate the drop deformation. We observe good agreement with the theory at low Ca and then the discrepancies get larger at higher Ca as expected. Our results are also in good agreement with the boundary-integral simulations of Stone and Leal [32].

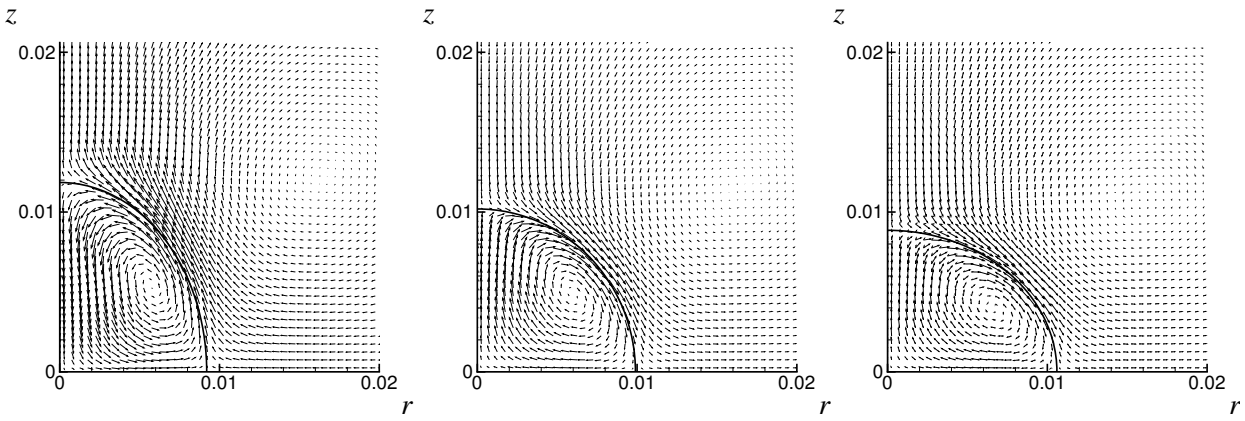

(a) Case A (b) Case B (c) Case C

FIG. 4. Drop deformation and induced flow pattern for $Ca_E = 0.4$ for the three typical cases given in Tab. I. Note that the velocity scale is different in the three figures.

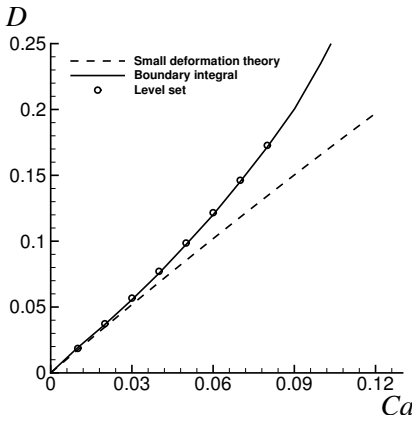

FIG. 5. Comparison of small deformation theory and numerical simulations for a drop stretching in linear flow.

TABLE II. The errors in the computed deformation compared to the solution for a grid size of $R/h = 160$.

R/h	$D_n - D_{160}$	Ratio
20	2.94×10^{-1}	-
40	9.21×10^{-2}	3.19
80	2.87×10^{-2}	3.21

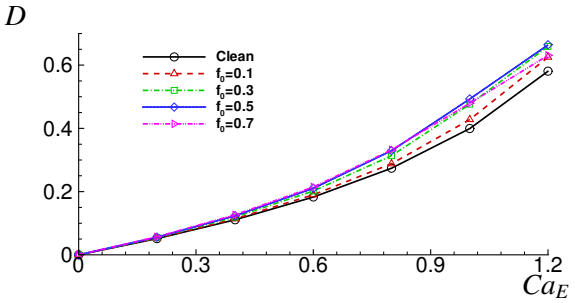

FIG. 6. (Color online) Case A. Deformation as a function of electric capillary number for various surfactant coverages.

3. Grid refinement study

Table II shows the results of a grid refinement study. Case C was computed with $Ca_E = 0.2$ and surfactant parameters $\Gamma_0 = 0.1$ and $\beta = 0.1$. The error in deformation is measured on three different grids, $R/h = 20, 40, 80$, and compared to a reference solution taken at a grid size of $R/h = 160$. We see that the ratio in errors is around 3. In Leveque and Li [33], it was argued that a qth order method should produce a ratio $(4^q - 1)/(2^q - 1)$ when the solution on a grid not much finer is used as the reference solution. A ratio of 3 indicates first-order convergence.

B. Influence of surfactants on steady-state deformation

We now turn our attention to the steady-state deformation of a drop with a surfactant present on the interface.

To limit the parameter space, we will consider the above cases A, B and C, and vary the electric capillary number and surfactant coverage. For the surfactant, we choose an elasticity of $\beta = 0.2$ and a surfactant Peclet number of $Pe = 10$. The Ohnesorge number is set to $Oh = 0.1$ and the viscosity ratio is set to unity unless otherwise noted.

1. Case A

We first study the effect of surfactants on the system with prolate deformation and counter-clockwise flow. The deformation as a function of electric capillary number for different surfactant coverages is shown in Fig. 6. For low Ca_E, higher surfactant concentrations lead to higher deformation. This is due to the induced flow which for this case is from the equator to the poles (see Fig. 4(a)). This will transport surfactant to the tip of the drop, which reduces interfacial tension

at the poles. Since there must be a balance between the normal interfacial-tension forces, the hydrodynamic pressure and the electric pressure, the drop extends more to yield a higher mean curvature. However, as the drop is stretched further, the average interfacial tension increases due to dilution of the surfactant. This will act to reduce deformation, and eventually this effect becomes stronger than the effect of reduced interfacial tension at the tips, leading to less deformation. This is clearly seen for $f_0 = 0.7$ in the figure. At low Ca_E, the deformation is higher than for the lower f_0 numbers, but at high Ca_E, it becomes lower.

In Figure 7 we illustrate the drop shapes and velocity patterns for electric capillary numbers 0.2, 0.8 and 1.2, and for a clean and surfactant-covered drop. We immediately see the reduced velocities for the surfactant-covered drop, which is due to the Marangoni stresses acting in the opposite direction to the electrically induced shear stresses. An important application area of electrically induced flow is enhanced mixing, for instance in heat exchangers. Here, we see that the presence of surfactants may significantly inhibit the internal circulation, and this may be important for industrial applications. Additionally, we observe that for the higher Ca_E, the velocities are larger near the tip of the drop. This leads to an increase in surfactant convection here. This is further illustrated in Figure 8, which shows the interfacial tension as a function of arc length, s, starting from the tip of the drop and moving in the clockwise direction. For low Ca_E, the interfacial tension follows a smooth S-curve, but for higher Ca_E, there is a sharper gradient near the drop pole and very little change near the equator.

In Figure 9, we plot the actual surfactant concentration for $Ca_E = 1.2$. At low concentrations, the area around the equator is nearly depleted, and then there is a sharp gradient towards the tip. However, since the concentration is low, this only leads to modest gradients in the interfacial tension as shown in Figure 8(c). At higher concentrations, the concentration at the tips approaches the maximum surfactant packing. This leads to larger gradients in the interfacial tension than for the low concentrations, and correspondingly higher Marangoni stresses which lead to more uniform surfactant profiles. The gradient of the interfacial tension, which is the main component of the Marangoni stresses, is shown in Figure 10 for $Ca_E = 1.2$. From this we see that the Marangoni stresses are largest in the area near the tip, where the convection is strongest, and that higher surfactant concentrations lead to higher Marangoni stresses.

2. Case B

Here, we consider the case where the drop deforms in a prolate fashion, but the induced flow is from the poles to the equator. The deformation as a function of electric capillary number for different surfactant coverages is shown in Fig. 11. We see that a higher concentration of surfactant consistently gives a lower degree of deformation. The reason for this is that now surfactant is swept towards the equator instead of the poles. The interfacial tension will therefore become higher at the tips, and give a larger resistance against deformation than for a clean drop.

Note that the deformation is relatively low for the Ca_E considered here. We would expect that dilatational effects would occur here as well for higher deformations. However, for this case these effects would only give an even lower deformation, further increasing the difference between the clean and surfactant-covered drops. We would also expect, as we will see in the next section, that the dilatational effects would occur sooner than for case A. This is because when surfactant is swept towards the equator instead of towards the poles, it will be spread over a larger surface area and thereby contribute less towards a change in the balance between capillary forces and electrical forces.

3. Case C

Next, we consider the case of oblate deformation, with induced flow from the poles to the equator. The deformation as a function of electric capillary number for different surfactant coverages is shown in Fig. 12. For the chosen parameter set, we see that the effect of surfactant is very small at low Ca_E. As shown in the closeup in Fig. 12(b), the deformation is slightly larger for increasing surfactant concentrations. This is again because surfactant is swept towards the drop equator by the induced flow, and the resulting low interfacial tension here gives a corresponding lower resistance towards deformation. The change in deformation is lower than in Case A because the surfactant now is spread across the equator instead of concentrated at the tips.

This also means that the relative effect of dilatation will occur earlier than for case A. This can be seen at higher Ca_E from Fig. 12. For higher Ca_E (but still low D compared to case A), the difference in deformation is completely reversed such that the clean drop has the highest deformation and the surfactant-covered drop with $f_0 = 0.7$ has the lowest deformation.

4. Influence of viscosity ratio

We end by presenting results on the influence of viscosity ratio. This parameter has proved to be an important parameter for the deformation of a drop in extensional flow. In Milliken and Leal[34] it was shown that smaller viscosity ratios gave a larger sensitivity to surfactant. We therefore rerun our previous simulations with a viscosity ratio of $\mu_r = 0.1$. The results for all three cases are presented in Figure 13. It is evident that the difference in deformation due to surfactants here is higher. The reason for this is that for higher viscosity ratios, the internal circulation is already retarded due to viscosity, and the contribution from the additional Marangoni stresses will become relatively smaller than for lower viscosity ratios. Since the circulation is higher here, more surfactant will be swept towards the tips and the change in deformation will be higher. The stronger Marangoni stresses at lower viscosity ratios also make the dilatational effects less prominent.

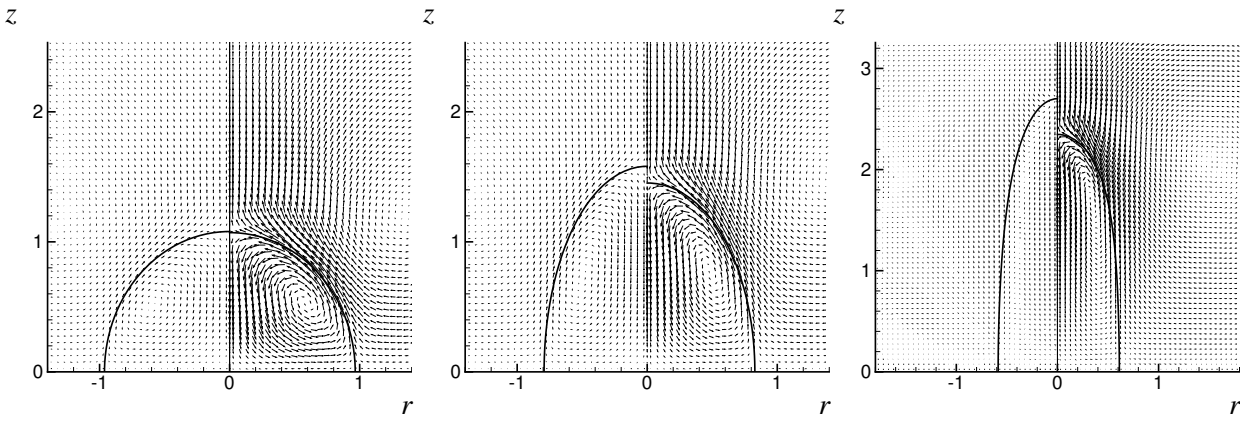

(a) $Ca_E = 0.2$ (b) $Ca_E = 0.8$ (c) $Ca_E = 1.2$

FIG. 7. Case A. Drop deformation and induced flow pattern. The right quadrant shows the clean drop and the left quadrant shows the surfactant-covered drop with $f_0 = 0.7$. The velocity scale is different in the three figures.

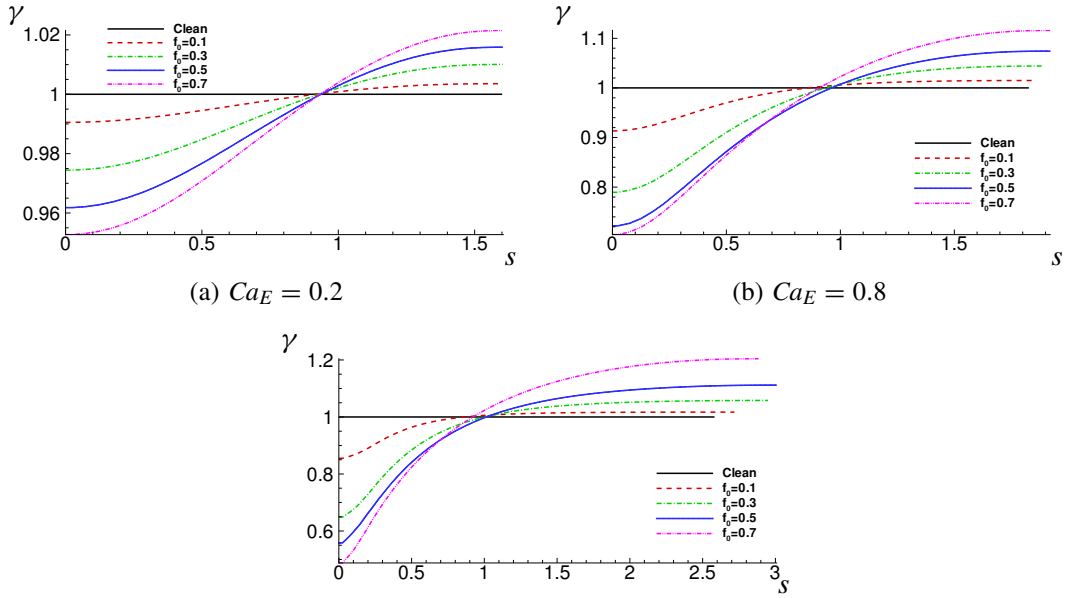

(a) $Ca_E = 0.2$ (b) $Ca_E = 0.8$

(c) $Ca_E = 1.2$

FIG. 8. (Color online) Case A. Interfacial tension along the interface for various surfactant coverages.

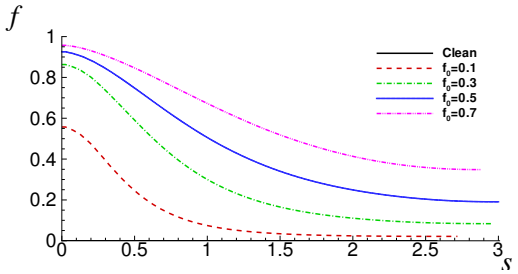

FIG. 9. (Color online) Case A. Surfactant concentration as a function of arc length for various surfactant coverages.

For instance, we see that for the oblately deformed drop, in Fig 13(c), that the deformation is now higher for higher surfactant coverages, even at high Ca_E.

IV. CONCLUSIONS

A level-set model for two-phase flows, coupled with models for electrohydrodynamic forces and surface-active agents was developed to investigate the influence of surfactants on the steady-state deformation of a drop in an electric field.

Leaky-dielectric fluids can deform into both prolate and oblate shapes, depending on the ratio of conductivities and permittivities. Additionally, the direction of the induced circulation can be both clockwise and counter-clockwise for the prolate shapes. It was found that for prolate deformation and counter-clockwise circulation, the presence of surfactant

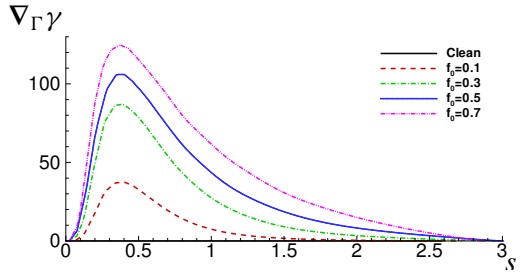

FIG. 10. (Color online) Case A. Gradient of interfacial tension as a function of electric capillary number for various surfactant coverages.

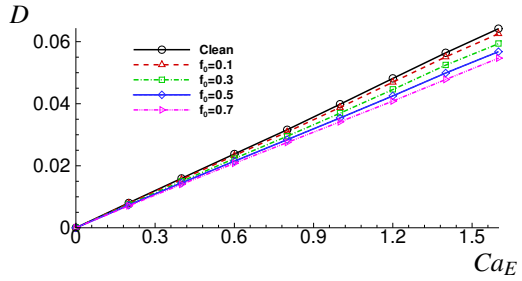

FIG. 11. (Color online) Case B. Deformation as a function of electric capillary number for various surfactant coverages.

leads to greater deformation at low surfactant concentrations. At high surfactant concentrations and high electric capillary numbers, however, the effect of surfactant dilution becomes stronger than the effect of reduced interfacial tension at the tips, and the deformation decreases. This behavior is similar to that of a drop in extensional flow.

For prolate deformation and clockwise flow, the surfactants are swept in the opposite direction, and cause a reduction in deformation. Although not shown here, it seems clear that dilatational effects will lead to an additional reduction in deformation for the surfactant-covered drop, and thereby increase the differences between the clean and surfactant-covered case further.

For oblate deformation, which always gives clockwise flow, the results are similar to that of prolate deformation and counter-clockwise flow, deformation is increased until dilatational effects start to dominate. However, this occurs earlier here, since the surfactant is not concentrated at the tips, but instead spread out over the equator of the drop. Finally, it was shown that for smaller viscosity ratios, the influence of surfactant is stronger, since the relative importance of the Marangoni stresses becomes higher.

In this work, only steady-state deformation was considered. At high electric capillary numbers, no steady state exists and the drop will stretch further and will eventually break up. It would be of interest to investigate the influence of surfactants on this breakup behavior. In particular, for a conductive drop in an otherwise dielectric medium, the influence of surfactant may be important even though it has no influence on the steady-state deformation. The presented numerical method is applicable to such a study as well.

ACKNOWLEDGMENTS

This work is funded by the project "Electrocoalescence – Criteria for an efficient process in real crude oil systems"; coordinated by SINTEF Energy Research. The project is supported by The Research Council of Norway, under the contract no: 169466/S30, and by the following industrial partners: Aker Solutions AS, BP Exploration Operating Company Ltd, Hamworthy Technology & Products AS, Petrobras, Saudi Aramco, Shell Technology Norway AS and Statoil ASA.

We thank the anonymous reviewers for their constructive comments.

[1] S. Laohalertdecha, P. Naphon, and S. Wongwises, "A review of electrohydrodynamic enhancement of heat transfer," Renew. Sustain. Energy Rev. **11**, 858–876 (2007).

[2] J. S. Eow and M. Ghadiri, "Electrostatic enhancement of coalescence of water droplets in oil: a review of the technology," Chem. Eng. J. **85**, 357–368 (2002).

[3] J. Sjöblom, N. Aske, I. H. Auflem, Ø. Brandal, T. E. Havre, Ø. Sæther, A. Westvik, E. E. Johnsen, and H. Kallevik, "Our current understanding of water-in-crude oil emulsions.: Recent characterization techniques and high pressure performance," Advances in Colloid and Interface Science **100-102**, 399–473 (2003).

[4] W. J. Milliken, H. A. Stone, and L. G. Leal, "The effect of surfactant on transient motion of Newtonian drops," Phys. Fluids A **5**, 69–79 (1993).

[5] Y. Pawar and K. J. Stebe, "Marangoni effects on drop deformation in an extensional flow: The role of surfactant physical chemistry. I. Insoluble surfactants," Phys. Fluids **8**, 1738–1751 (1996).

[6] Charles D. Eggleton and Kathleen J. Stebe, "An adsorption-desorption-controlled surfactant on a deforming droplet," J. Colloid Interface Sci. **208**, 68–80 (1998).

[7] Charles D. Eggleton, Yashodhara P. Pawar, and Kathleen J. Stebe, "Insoluble surfactants on a drop in an extensional flow: a generalization of the stagnated surface limit to deforming interfaces," J. of Fluid Mech. **385**, 79–99 (1999).

[8] X. Li and C. Pozrikidis, "The effect of surfactants on drop deformation and on the rheology of dilute emulsions in Stokes flow," J. of Fluid Mech. **341**, 165–194 (1997).

[9] M.-C. Lai, Y.-H. Tseng, and H. Huang, "An immersed boundary method for interfacial flows with insoluble surfactant," J. Comput. Phys. **227**, 7270–7293 (2008).

[10] C. D. Eggleton, T. Tsai, and K. J. Stebe, "Tip streaming from a drop in the presence of surfactants," Phys. Rev. Lett. **87**, 048302 (2001).

[11] R. A. De Bruijn, "Tipstreaming of drops in simple shear flows," Chem. Eng. Sci. **48**, 277–284 (1993).

[12] Y. Y. Renardy, M. Renardy, and V. Cristini, "A new volume-of-fluid formulation for surfactants and simulations of drop deformation under shear at a low viscosity ratio," Eur. J. Mech. B Fluids **21**, 49–59 (2002).

[13] K. E. Teigen, P. Song, J. Lowengrub, and A.Voigt, "A diffuse-interface method for two-phase flows with soluble surfactants," J. Comput. Phys. (2010), Accepted.

[14] G. I. Taylor, "Studies in electrohydrodynamics I. the cirulation produced in a drop by an electric field," Proc. R. Soc. A **291**, 159–166 (1966).

[15] J. R. Melcher and G. I. Taylor, "Electrohydrodynamics: A review of the role of interfacial shear stresses," Annu. Rev. Fluid Mech. **1**, 111–146 (1969).

[16] J. Ha and S. Yang, "Effect of nonionic surfactant on the deformation and breakup of a drop in an electric field," J. Colloid and Interface Sci. **206**, 195–204 (1998).

[17] Mark Sussman, Peter Smereka, and Stanley Osher, "A level set approach for computing solutions to incompressible two-phase flow," J. Comput. Phys. **114**, 146–159 (1994).

[18] Stanley Osher and Ronald Fedkiw, *Level set methods and dynamic implicit surfaces* (Springer, New York, 2003).

[19] G. Tomar, D. Gerlach, G. Biswas, N. Alleborn, A. Sharma, F. Durst, S. W. J. Welch, and A. Delgado, "Two-phase electrohydrodynamic simulations using a volume-of-fluid approach," J. Comput. Phys. **227**, 1267–1285 (2007).

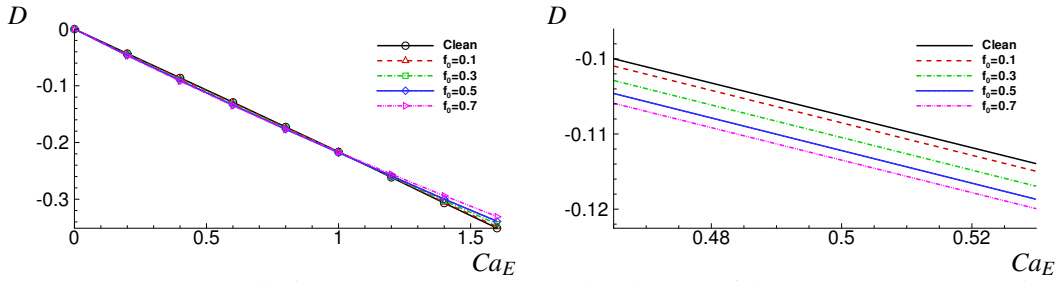

(a) Full view (b) Close up of the curves near $Ca_E = 0.5$.

FIG. 12. (Color online) Case C. Deformation as a function of electric capillary number for various surfactant coverages.

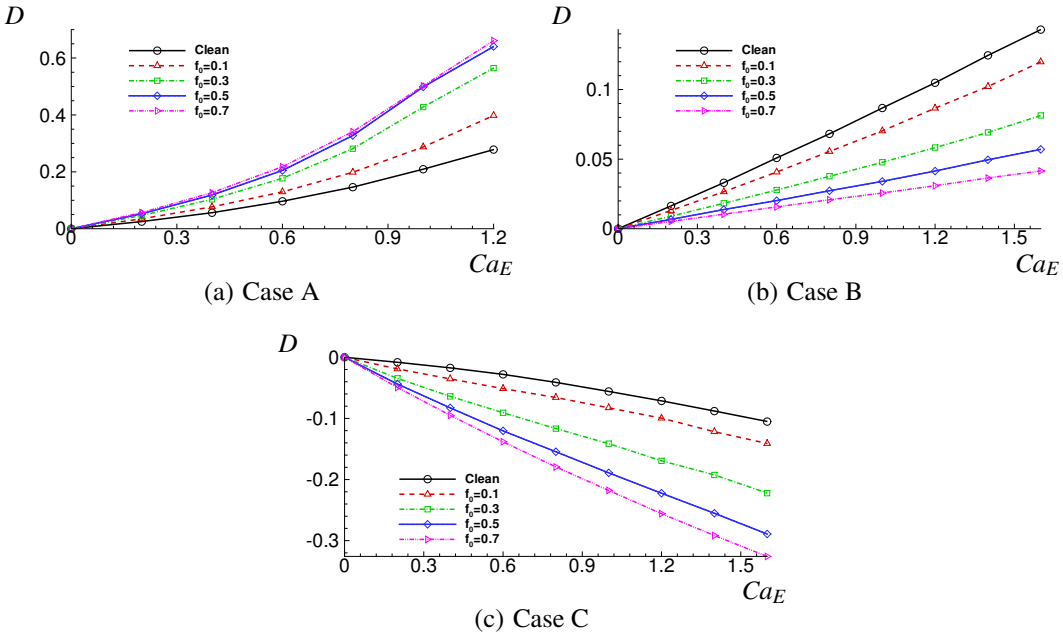

(a) Case A (b) Case B

(c) Case C

FIG. 13. (Color online). Deformation as a function of electric capillary number for various surfactant coverages at viscosity ratio $\mu_r = 0.1$.

[20] J. J. Xu and H. Zhao, "An Eulerian formulation for solving partial differential equations along a moving interface," J. Sci. Comp. **19**, 573–594 (2003).

[21] J. J. Xu, Z. Li, J. Lowengrub, and H. Zhao, "A level set method for interfacial flows with surfactant," J. Comp. Phys. **212**, 590–616 (2006).

[22] H. K. Zhao, T. Chan, B. Merriman, and S. Osher, "A variational level set approach to multiphase motion," J. Comput. Phys. **127**, 179–195 (1996).

[23] D. Adalsteinsson and J.A. Sethian, "The fast construction of extension velocities in level set methods," J. Comput. Phys. **148**, 2–22 (1999).

[24] G. S. Jiang and D. Peng, "Weighted ENO schemes for Hamilton–Jacobi equations," SIAM J. Sci. Comput. **21**, 2126–2143 (2000).

[25] J. F. B. M. Kraaijevanger, "Contractivity of Runge-Kutta methods," BIT **31**, 482–528 (1991).

[26] D. I. Ketcheson and A. C. Robinson, "On the practical importance of the SSP property for Runge-Kutta time integrators for some common Godunov-type schemes," Int. J. Numer. Meth. Fluids **48**, 271–303 (2005).

[27] Y. Renardy and M. Renardy, "PROST: A parabolic reconstruction of surface tension for the volume-of-fluid method," J. Comput. Phys. **183**, 400–421 (2002).

[28] O. O. Ajayi, "A note on Taylor's electrohydrodynamic theory," Proc. R. Soc. Lond. A **364**, 499–507 (1978).

[29] J. Q. Feng and T. C. Scott, "A computational analysis of electrohydrodynamics of a leaky dielectric drop in an electric field," J. Fluid. Mech. **311**, 289–326 (1996).

[30] J. Hua, L. K. Lim, and C. Wang, "Numerical simulation of deformation/motion of a drop suspended in viscous liquids under influence of steady electric fields," Phys. Fluids **20**, 113302 (2008).

[31] E. Lac and G. M. Homsy, "Axisymmetric deformation and stability of a viscous drop in a steady electric field," J. Fluid Mech. **590**, 239–264 (2007).

[32] H. A. Stone and L. G. Leal, "The effect of surfactants on drop deformation and breakup," J. Fluid. Mech **220**, 161–186 (1990).

[33] R. J. Leveque and Z. Li, "The immersed interface method for elliptic equations with discontinuous coefficients and singular sources," SIAM J. Numer. Anal. **31**, 1019–1044 (1994).

[34] W. J. Milliken and L. G. Leal, "The influence of surfactant on the deformation and breakup of a viscous drop-the effect of surfactant solubility," J. Colloid and Interface Sci. **166**, 275–285 (1994).